La mer 38 : 233-243, 2000
Société franco-japonaise d'océanographie, Tokyo

Several aspects of the simulated response of the Japan (East) Sea to synoptic atmospheric forcing due to siberian cold air outbreaks

Christopher N.K. MOOERS*, HeeSook KANG*, and Shuyi S. CHEN**

Abstract : The Japan (East) Sea (JES) is influenced by synoptic-scale Siberian cold air outbreaks during the winter season. The response of JES to two cold-air outbreaks in early January 1997 is explored with numerical simulations using synoptic winds from ECMWF, NSCAT, and MM5 to drive a mesoscale eddy-admitting JES circulation model (JES-POM). The importance of the associated low level wind jet (and the consequent high heat loss region) off Vladivostok is demonstrated. The simulated response includes cooling in the upper layer and low-order, barotropic, basin-scale divergence and vorticity modes. The net response is not very sensitive to the spatial and temporal resolution of the wind-forcing; however, the synoptic sequence of the response is quite sensitive.

Key words : *ocean circulation, semi-enclosed sea, cold air outbreak, atmospheric forcing*

1. Introduction

The circulation of the Japan (East) Sea (JES) is driven mainly by the throughflow of the Tsushima Warm Current and atmospheric forcing, including Siberian cold air outbreaks associated with the passage of extratropical cyclones and fronts, on a 4-to-10 day timescale, during the winter season (typically late November through early March). The response of the JES to cold air outbreaks is anticipated to be complex, ranging from increased sea states to wind-driven setup (along the Japanese coast) and setdown (along the Korean and Russian coasts) of coastal sea level; to intense mixing, cooling, and evaporation on the Asian side of the JES, plus adjustment to intense precipitation on the Japanese side; and to generation of transient open ocean and coastal upwelling/downwelling, near-inertial motions, and mixed-layer deepening. However, most previous studies (a notable exception is BANG *et al.* (1996)) of JES oceanic responses to atmospheric forcing have used climatological monthly or mean fields which, of course, do not include the synoptic effects of individual winter storms that dominate the mean fields as well as the variability. The availability of high resolution surface winds from satellite scatterometer measurements and mesoscale numerical weather prediction models now allows addressing these response issues in new ways, as described below.

The interaction of the cold air outbreak driven JES transient response with the JES general circulation is thought to be essential for wintertime ventilation of the JES and the annual formation of intermediate water and occasional formation of deep water (cf. SENJYU and SUDO, 1996). Observational evidence suggests that the center of intense air-sea interaction and ventilation is located off Vladivostok (cf. SEUNG and YOON, 1995) (though there are alternative candidate sites and mechanisms), where a low-level jet (associated with cold air outbreaks) flows seaward through a prominent coastal valley north of Vladivostok. This hypothesis and related issues are explored by

* OPEL/AMP/RSMAS/University of Miami
4600 Rickenbacker Causeway
Miami, FL 33149-1098 USA
Email: cmooers@rsmas.miami.edu
** MPO/RSMAS/University of Miami
4600 Rickenbacker Causeway
Miami, FL 33149-1098 USA

driving a regional ocean circulation model (JES-POM) with various surface wind datasets derived from a standard operational NWP model (ECMWF), a spaceborne scatterometer (NSCAT/ADEOS), and an atmospheric mesoscale circulation model (the PSU/NCAR MM5). Examples are presented of the simulated responses, and of their sensitivity to the various atmospheric forcing fields utilized. This study complements an earlier analysis (KAWAMURA and WU, 1998) of somewhat similar issues (but for mean conditions over the entire month of January) with air-sea transfer estimates (using NSCAT winds) and satellite-sensed sea surface temperature (SST) fields.

The JES response to the cold air outbreaks is simulated with JES-POM (KANG, 1997), an implementation of the Princeton Ocean Model (POM, BLUMBERG and MELLOR, 1987) for the JES. POM is a primitive equation model with a free seasurface, as well as many other important attributes. The version of JES-POM used here has 26 sigma levels and ca. 10 km horizontal resolution; it uses a value of HORCON = 0.1 in the Smagorinsky lateral turbulence parameterization. The model was spun-up for 4,200 days with the Na climatological mean winds (NA *et al.*, 1992), relaxation (time scale = 100 days) of surface temperature and salinity to the LEVITUS climatological means (LEVITUS, 1982), and specified throughflow of 2.8 Sv. (Note: the model was usefully in statistical equilibrium at that stage; otherwise, there was no particular reason for starting the synoptic forcing simulations at that time.) For the MM5 case, the wind-forcing and surface thermal forcing were replaced with MM5 winds and heat flux by ramping-up over five inertial periods (i.e., a total of 85 h) to the MM5 forcing of 00Z/1 JAN 97. For the NSCAT and ECMWF cases, the NSCAT and ECMWF winds, respectively, were used with the MM5 heat flux.

The PSU/NCAR (nonhydrostatic) atmospheric mesoscale model MM5 (DUDHIA, 1993) was implemented with a triply nested domain. The outer domain covers Northeast Asia and has 45-km horizontal resolution; the intermediate domain covers JES and its coastal areas and has 15-km resolution; and the inner domain covers an area off Vladivostok and has 5-km resolution. This implementation has 26 sigma levels between the surface and the 50 mb isobaric surface. MM5 is forced by the ECMWF global analysis fields on its lateral boundaries. A mesoscale analysis dataset including additional station observations is assimilated into the outer domain. The MM5 simulation has been verified by independent datasets; e.g., the GMS-5 satellite visible and infrared imagery and the JMA meteorological buoy near Oki Is. In the present study, fields from the intermediate domain (with 15-km resolution and no additional data assimilation) are used to force JES-POM.

2. Synoptic atmospheric conditions, 1 to 10 January 1997

Two extratropical cyclone (storm) passages occurred in JES during 1 to 10 January 1997 (Fig. 1). The first cyclone developed in association with a strong upper-level disturbance moving from Northeast Asia across the northern JES during 1 to 2 JAN, intensified, and

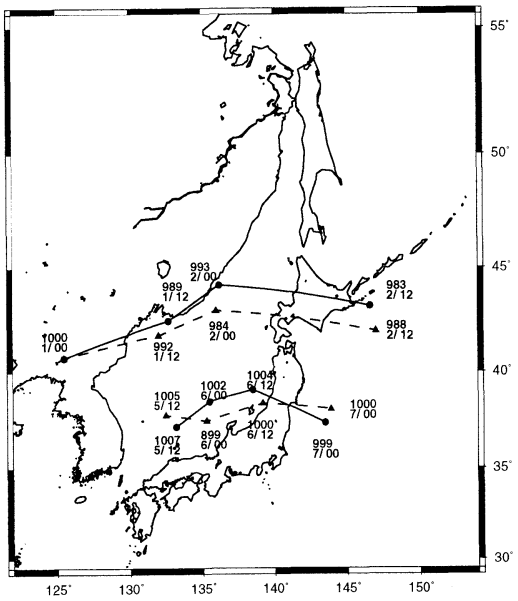

Fig. 1. Tracks of the cyclone centers associated with the two cold air outbreaks, 1 to 10 JAN 97. Centers are plotted every 12 hours from two sources: MM5 model (dashed line) and composite (solid line) of satellite visible and infrared imagery. (Center positions are labelled with central pressure (mb), day in JAN, and time (hours/GMT).)

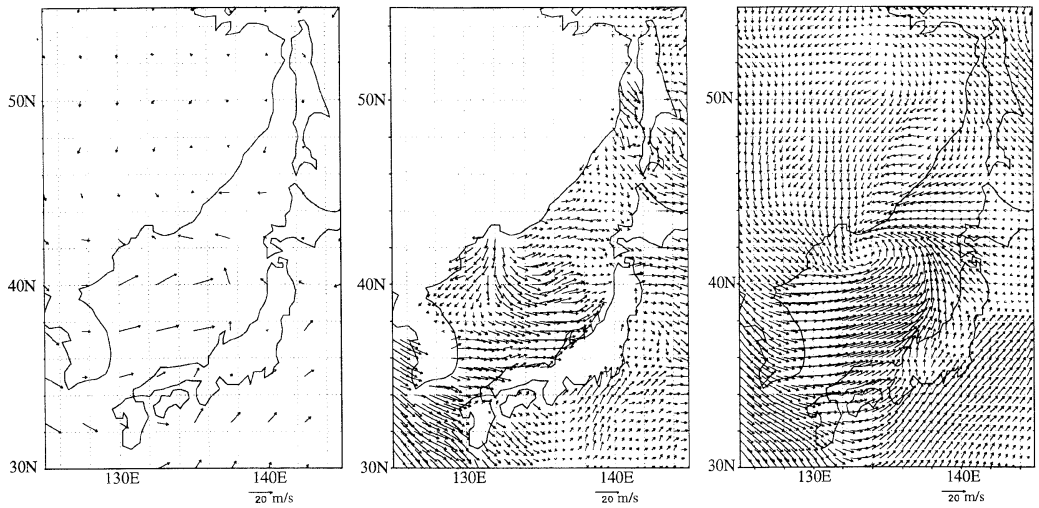

Fig. 2. Synoptic surface windfields for 12Z, 1 JAN 97 (left: ECMWF wind; center: NSCAT wind; right: MM5 wind).

moved rapidly more or less along the western side of the JES before crossing over northern Japan. The second cyclone developed in the southern JES during 5 to 6 JAN, intensified to a lesser degree, and moved slowly more or less along the eastern side of the JES (along a track ca. 500 km to the south of the first, and parallel to it) before crossing over central Japan. While the first storm can be categorized as a classical "cold air outbreak", the second storm lacked a strong outflow of cold air from Siberia and provided mostly wind-forcing.

3. The atmospheric forcing

Three sources of synoptic surface winds (noted above) were utilized for forcing JES-POM. Simultaneous "snapshots" of the three surface wind fields (Fig. 2) serve to indicate their differing attributes. For example, the ECMWF product has a resolution of 12 hrs and ca. 275 km; NSCAT has a resolution of 12 hrs and ca. 50 km; and MM5 has a resolution of 1 hr and 15 km. The three wind fields generally agree on the basin-scale; however, while the ECMWF wind field broadly indicates a cyclonic feature over the central JES, it (understandably) does not depict the seaward wind jet streaming from Vladivostok as indicated by NSCAT and MM5 fields. Further, the NSCAT field does not depict the low-level cyclonic circulation associated with the first storm that MM5 indicates, which has been validated independently with satellite visible and infrared imagery. The flow pattern of the nine-day mean surface wind stress fields (Fig. 3) of MM5, ECMWF, and NSCAT appear largely in agreement, and the maximum stress (ca. 0.2 N/m^2 in each case) occurs south of Vladivostok. However, from their difference fields (not shown) there are patterned differences with typical maximum magnitudes of 0.1 N/m^2 south of Vladivostok. The ECMWF and MM5 mean wind stress fields generally disagree significantly only within ca. 200 km of the coast due to MM5's superior resolution of coastal orography. Their significant differences with NSCAT wind stress are more widespread but greatest off Vladivostok. Also, their standard deviation fields (Fig. 4) are indicative of substantial differences in the underlying six hourly synoptic fields. The consequences for JES circulation of these differences in the forcing fields will be examined below.

The MM5 heat flux pattern is also of interest because it is used in the present simulations and is critical to water mass transformations. The 9-day mean heat flux (Fig. 3) indicates regions in excess of 900 W/m^2 oceanic heat loss off Vladivostok, in the southernmost JES, and along the coast of Honshu. The 9-day standard deviation of the heat flux (Fig. 4) indicates values of about 300 W/m^2 in the areas of

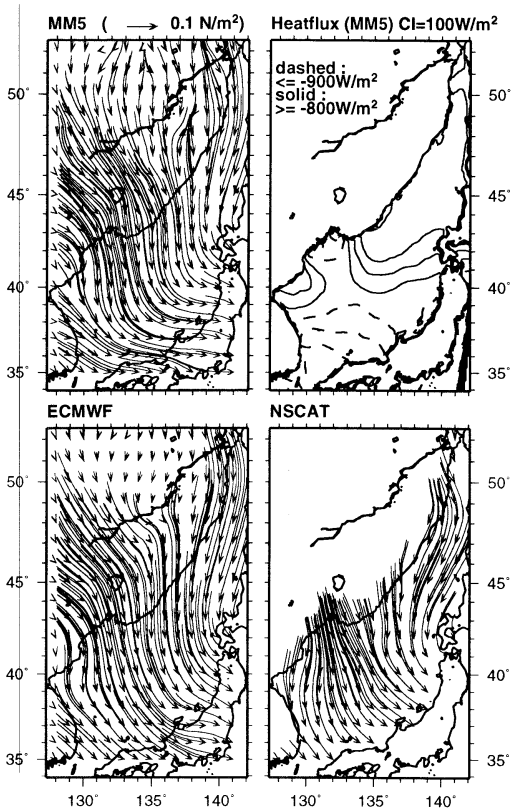

Fig. 3. Mean (1 to 10 JAN 97) of wind stress (N/m^2) from MM5, ECMWF, and NSCAT and of heat flux (W/m^2) from MM5.

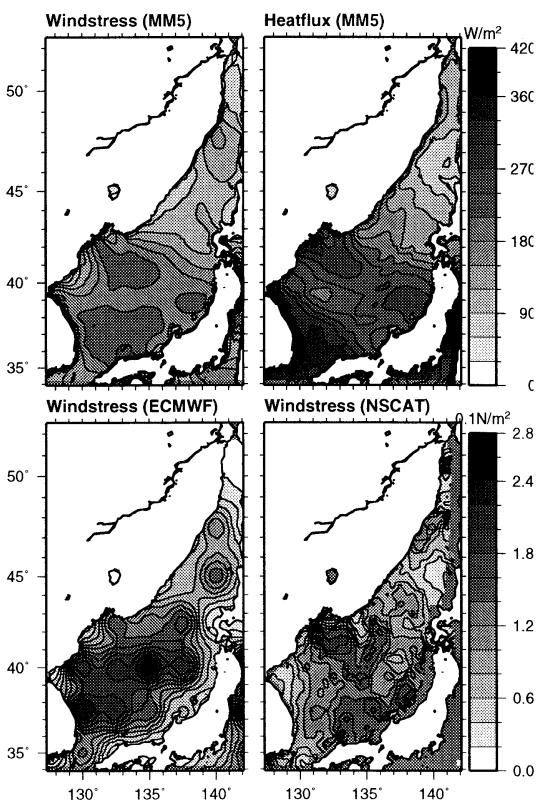

Fig. 4. Standard deviation (1 to 10 JAN 97) of wind stress (N/m^2) from MM5, ECMWF, and NSCAT and of heat flux (W/m^2) from MM5.

maximum heat loss, reflecting the intense synoptic variability.

4. The simulated JES response

Here, the focus is on the changes in seasurface height (SSH) and transport stream function (TSF) fields. The SSH field represents the barotropic divergence field, and the TSF field represents the barotropic vorticity field. Thus, the temporal variations of the SSH and TSF fields are related to the barotropic divergence and vorticity modes, respectively, of the JES basin.

The simulated 9-day mean SSH with MM5 forcing (Fig. 5) indicates the several main features of the upper layer general circulation of the JES: the East Korean Warm Current (EKWC) and its separation at 37.5 N, the meandering Subpolar Jet, the Nearshore Branch off Honshu, the cyclonic recirculation gyre off Wonsan Bay, the large recirculation cyclonic gyre over the Japan Basin, and a cyclonic gyre in the northern JES. The 9-day SSH standard deviation (Fig. 5) has a primary maximum in the northernmost JES and a secondary maximum in the southernmost JES, with typical values in the southern JES of 2 to 4 cm. The 9-day mean TSF (Fig. 5) indicates the throughflow transport from Korea Strait to Tsugaru and Soya Straits, plus the cyclonic recirculation gyres off Wonsan Bay and over the Japan Basin. The 9-day TSF standard deviation (Fig. 5) has a maximum (in excess of 3 Sv) over Yamato Rise and Japan Basin. Consequently, the spatial distribution of variability in TSF is opposite to that in SSH; i.e., high in the center and high in the north and south, respectively.

To assess the difference in the JES responses, the changes in SSH and TSF between 1 and 10

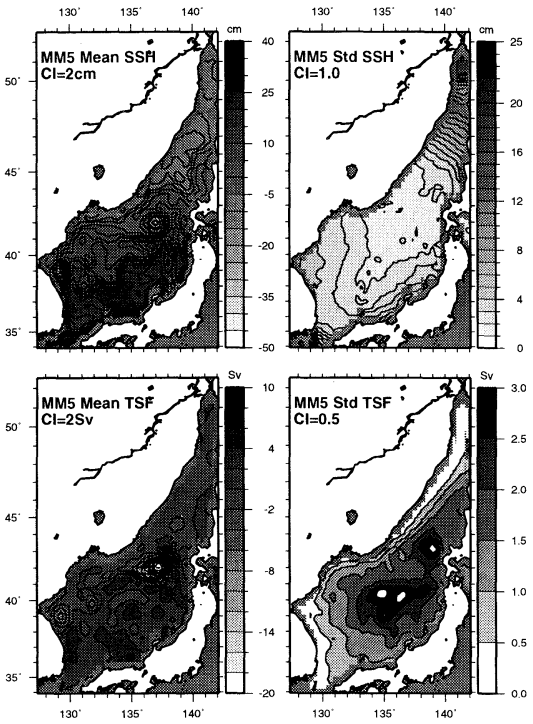

Fig. 5. Mean and standard deviation (1 to 10 JAN 97) of SSH and TSF for the MM5 case.

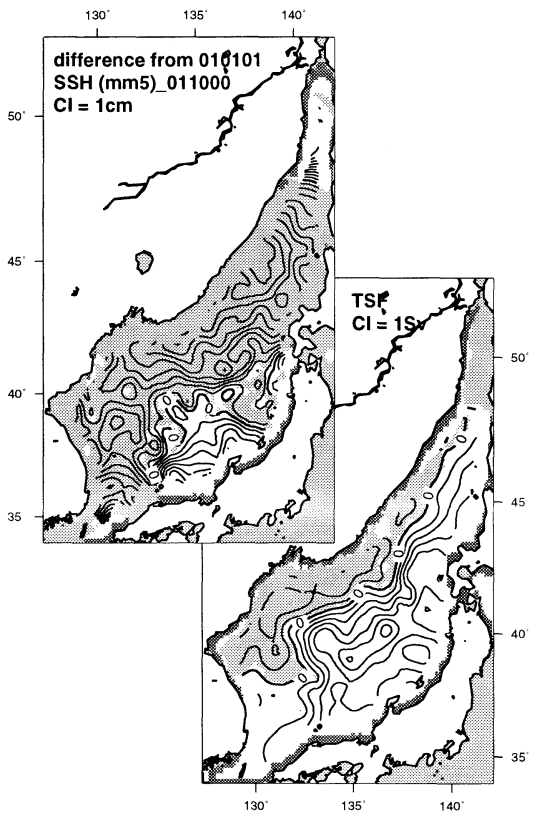

Fig. 6. SSH and TSF difference fields for 10 JAN -1 JAN 97 for the MM5 case. (Shaded area represents negative values)

January 1997 are compared for the three wind forcing fields. For conciseness, only the MM5 case is shown (Fig. 6). The SSH is setup and setdown by ca. 0.1 m in the south and north, respectively, in all three cases. However, the ECMWF and NSCAT (not shown) cases indicate a setup along the coast of North Korea and southern Russia, while the MM5 case indicates a setup along the coast of southwestern Japan, as expected. The TSF is increased and decreased by a few Sverdrups in the east and west, respectively, in all three cases. Moreover, their basin-scale patterns are very similar and suggestive of a response composed of basin scale modes, and they are each characterized by numerous mesoscale features. The temporal evolution of SSH and TSF needs further scrutiny, as given below.

To explore the nature of the dynamical response, tendencies in the barotropic divergence (SSH) and barotropic vorticity (TSF) fields are examined. The SSH and TSF difference fields (between several fiducial times given below) for the MM5 case (Figs. 7 and 8, resp.) indicate a finer temporal resolution analysis of the simulated fields, as given in the next section with EOFs, to characterize better the nature of the temporal variability. These fields were evaluated for the beginning of storm 1 minus start of synoptic run (12Z/1 JAN-01Z/1 JAN), end of storm 1 minus beginning of storm 1 (00Z/3 JAN-12Z/1 JAN), beginning of storm 2 minus end of storm 1 (06Z/5 JAN-00Z/3 JAN), end of storm 2 minus beginning of storm 2 (00Z/7 JAN-06Z/5 JAN), and stop of synoptic run minus end of storm 2 (00Z/10 JAN-00Z/7 JAN).

As measures of the sensitivity of the simulated response to the wind-forcing, the SSH and TSF difference fields for the NSCAT minus MM5 cases (Figs. 9 and 10, respectively) and ECMWF minus MM5 cases (not shown) are examined for the fiducial times utilized above.

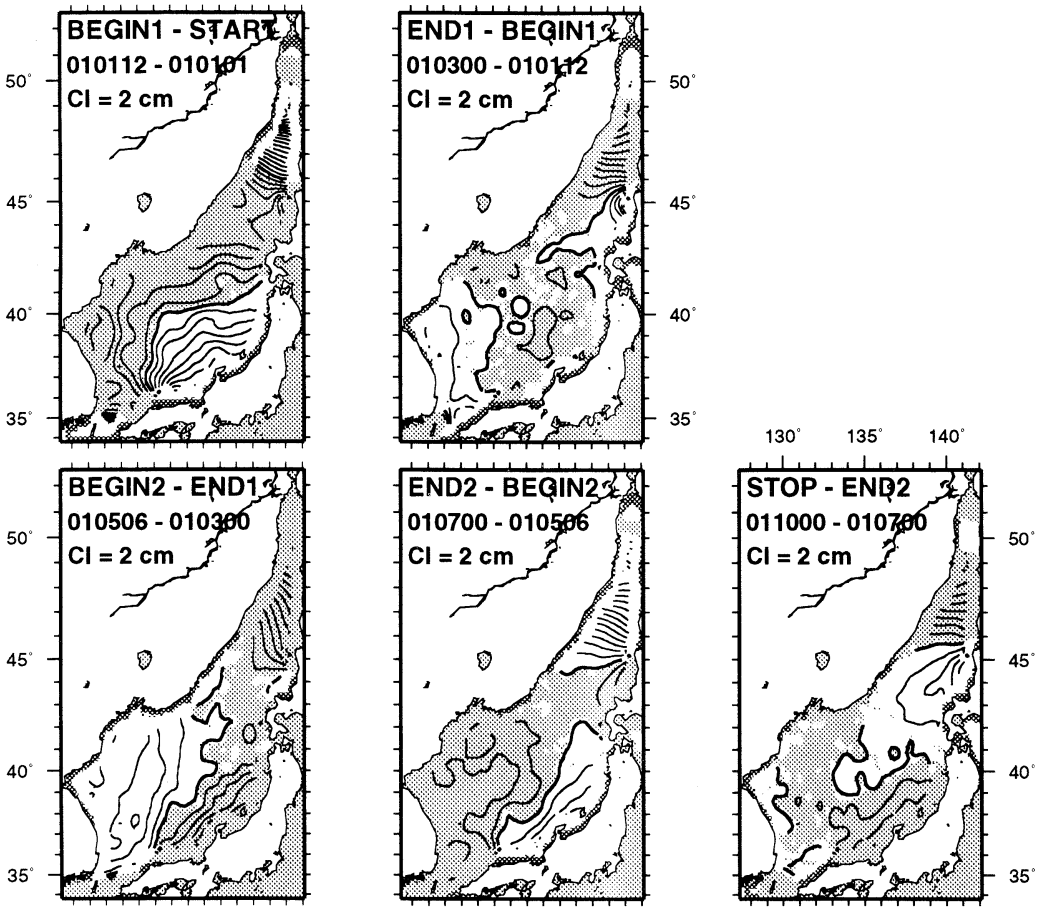

Fig. 7. SSH difference fields for the MM5 case. (Shaded area represents negative values)

Clearly, there are instantaneous basin-scale differences of order ±0.1m in SSH and ±6 Sv in TSF which, however, are substantially attenuated by the end of the calculations. (The patterns and magnitudes of the differences for the ECMWF minus MM5 cases (not shown) are very similar to those of NSCAT minus MM5 cases.) Thus, the calculated responses are very sensitive to the synoptic forcing used, though the "correct" forcing and response are not known and the attributes of ECMWF and NSCAT that lead to these differences have not been isolated.

While the emphasis here is on some aspects of the dynamical response, one aspect of the thermohaline response is examined, too, viz., the upper ocean thermal response at 41.5 N, 133.0 E. This position is located in the hypothesized Japan Sea Proper Water formation region (SENJYU and SUDO, 1996) and the designated "flux center" (KAWAMURA and WU, 1998), i.e., north of 41 N and between 132 and 134 E, as highlighted by previous authors (e.g., SEUNG and YOON, 1995). The temperature anomaly of the upper 100 m (Fig. 11) for the MM5 case indicates a rapid cooling in the upper 40 m during passage of the first cyclone and gradual cooling during the remainder of the period. While the SST decreased by a total of 0.9 C, the cooling depth increased to nearly 100 m, which is consistent with previous estimates for cooling due to cold air outbreaks in this region (e.g., KAWAMURA and WU, 1998). The cooling at this location for the NSCAT and ECMWF cases (not shown) was similar in SST decrease (also ca. 0.9 C). However, the cooling

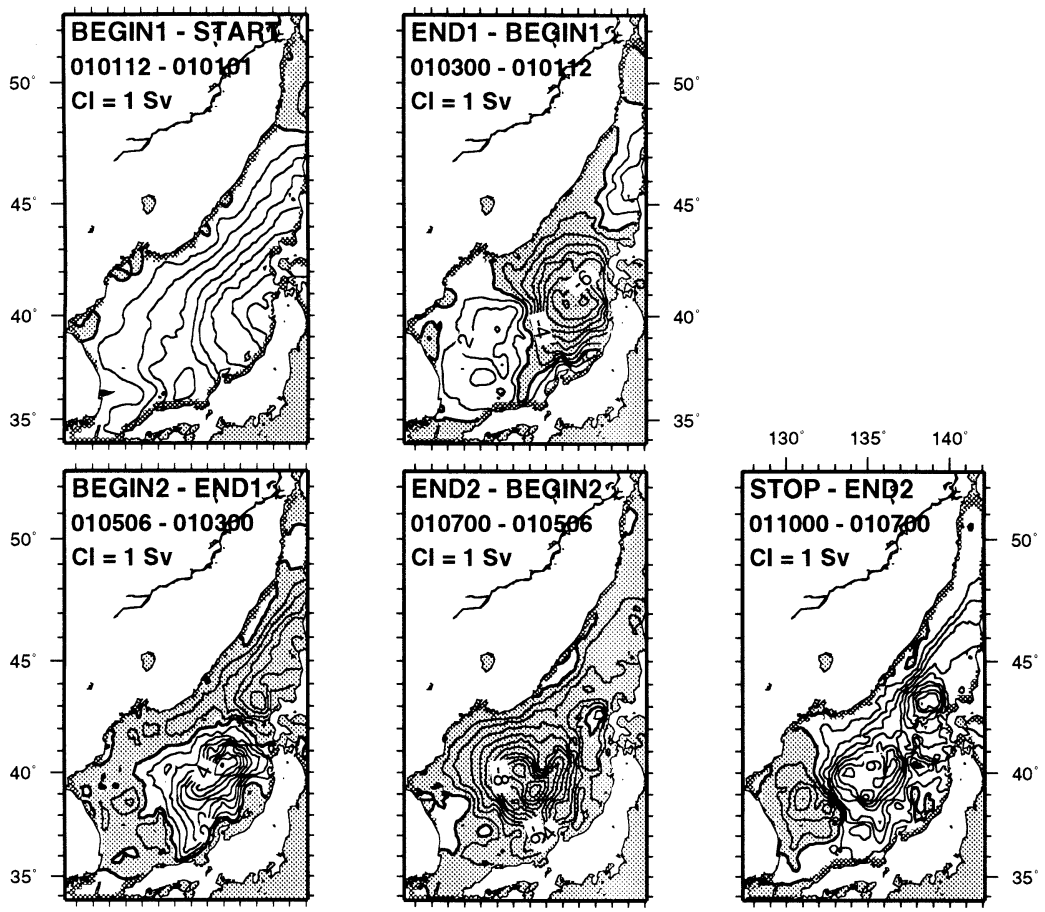

Fig. 8. TSF difference fields for the MM5 case. (Shaded area represents negative values)

depth was nearly 150 m for NSCAT and more than 150 m for ECMWF cases. These case-dependent differences in cooling response may become significant for longer integrations. The cooling response was highly spatially dependent (not shown) in the "flux center"; for example, at 42.5 N, 133.0 E, the cooling penetrated to 300 m while it was mainly confined to the upper 50 and 30 m at 41.5 N, 135.0 E and 42.5 N, 135.0 E (not shown), resp., in the MM5 case. The spatial variations in cooling response of the NSCAT and ECMWF cases were qualitatively similar to those of the MM5 case at these locations.

5. EOF Analyses

To efficiently characterize the space-time dependence of the transient response to the two cold air outbreaks, EOF analyses of 6-hourly gridded (subsampled by 1/3) SSH and TSF fields are presented for the MM5 case.

For SSH, the first four EOFs account for 70.8% of the variance. The spatial patterns of EOF1 and 4 (Fig. 12) are similar in the southern JES: when SSH is high along the Korean and southern Russian coasts, it is low along the Honshu coast; thus, they are basically zonal modes. The amplitudes (Fig. 13) are dominated by the weekly time scale and are in quadrature. Similarly, the spatial patterns of EOF 2 and 3 (Fig. 12) are similar throughout the JES except in the Korea (Tsushmia) Strait: when SSH is high in the southern basin it is low in the northern basin; thus, they are basically meridional modes. The amplitudes (Fig. 13) are dominated by the daily time scale,

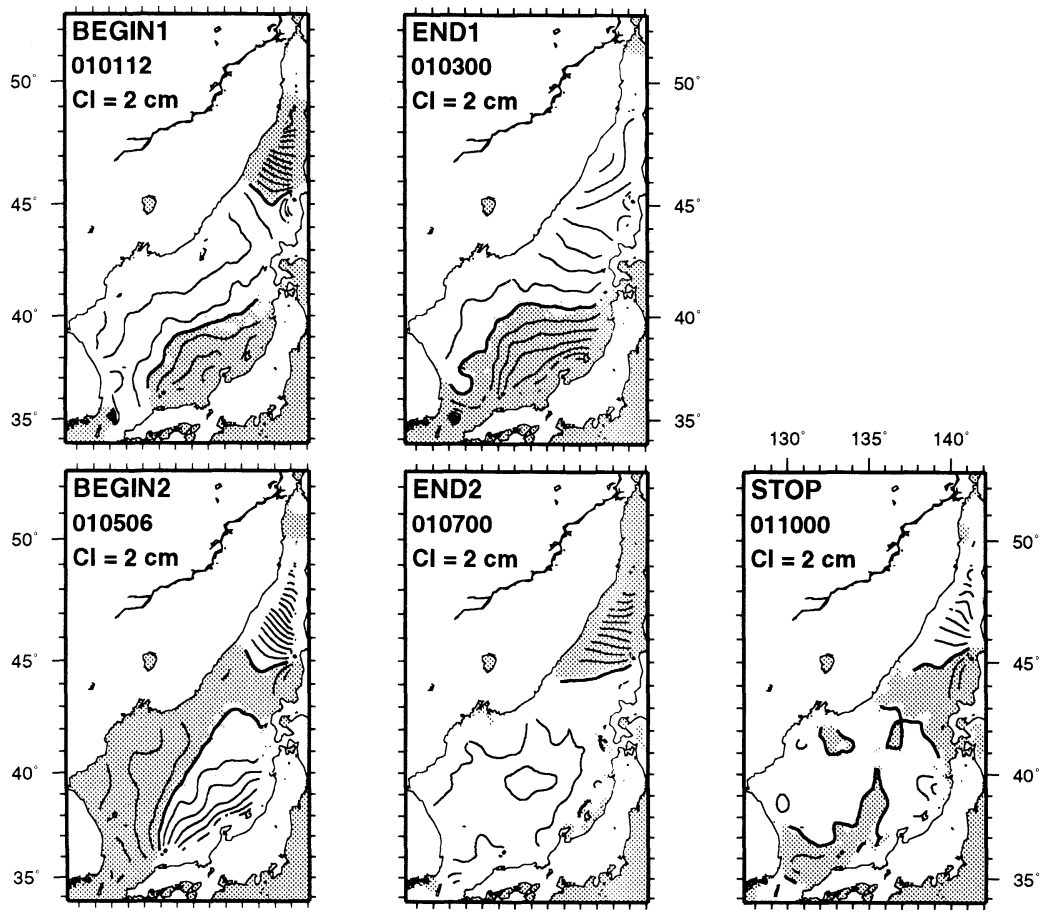

Fig. 9. SSH difference fields for the MM5-NSCAT cases. (Shaded area represents negative values)

which is due to aliasing of near-inertial energy. There is not a simple phase relation between their amplitudes except immediately after the passage of the first and second storms when they are in-phase.

For TSF, the first four EOFs account for 84.5% of the variance. The spatial patterns of EOF 1, 2, 3, and 4 all have a different character (Fig. 14). EOF 1 is in-phase throughout the basin, with an antinode over the Yamato Rise and Japan Basin; EOF 2 is basically a meridional mode, EOF 3 is basically a zonal mode, and EOF 4 is a sub-basin-scale mode. The EOF 1 amplitude (Fig. 15) is dominated by a strong reversal (change of sign) event associated with the passage of the second cyclone. There is a secondary fluctuation associated with the aliased near-inertial motion. The EOF 2 and 3 amplitudes are dominated by impulses of opposite sign associated with the passages of the two cyclones, and they are in quadrature. The EOF 4 amplitude is dominated by positive pulses associated with each cyclone passage and a strong reversal event during the final relaxation phase.

6. Summary

While the net change in barotropic vorticity (TSF) over nine days is not very sensitive to the differences in the three wind-forcing fields, the net change in barotropic divergence (SSH) is more sensitive to the choice of forcing. The synoptic response includes several basin-scale, barotropic vorticity and divergence modes. The modal amplitudes primarily vary with the timescale of the cold air outbreaks, but some

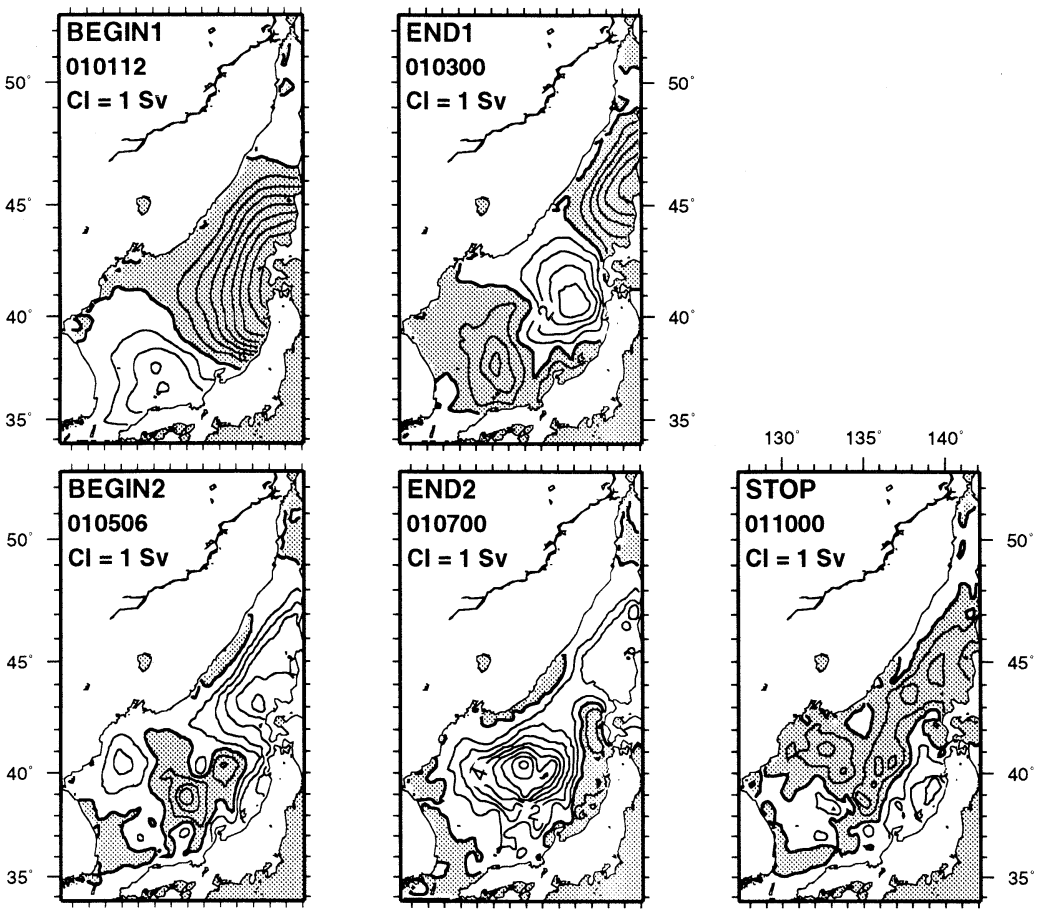

Fig. 10. TSF difference fields for the MM5-NSCAT cases. (Shaded area represents negative values)

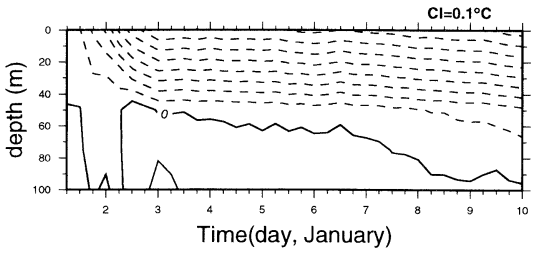

Fig. 11. Time-depth plot of temperature differences relative to the first temperature profile at 41.5N, 133E, 1 to 10 JAN 97 for the MM5 case. (Dashed lines represent negative values, cooling)

secondarily vary with a near-inertial period. These modes are intense enough that they should be detectable in time series of observations and synoptic maps. The cooling response of the upper ocean in the "flux center" off Vladivostok is consistent with this being a region where the seasonal succession of cold air outbreaks produces significant convection and ventilation. These issues will be pursued further with longer simulations. Overall, the sensitivity in temporal evolution for different forcing fields indicate that it is useful to utilize a data-assimilative atmospheric mesoscale model (e.g., the PSU/NCAR MM5) for accurate estimations of the atmospheric forcing associated with cold air outbreaks and the simulation of the response of JES to them.

Acknowledgement

This research was sponsored by the Navy Ocean Modeling and Prediction (NOMP) Program and the Departmental Research Initiative

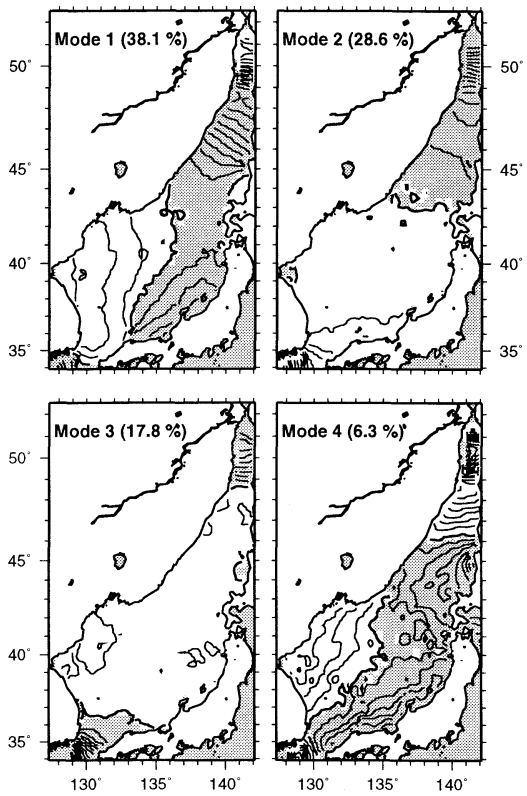

Fig. 12. Spatial patterns for first four SSH EOFs for the MM5 case. (Shaded area represents negative values)

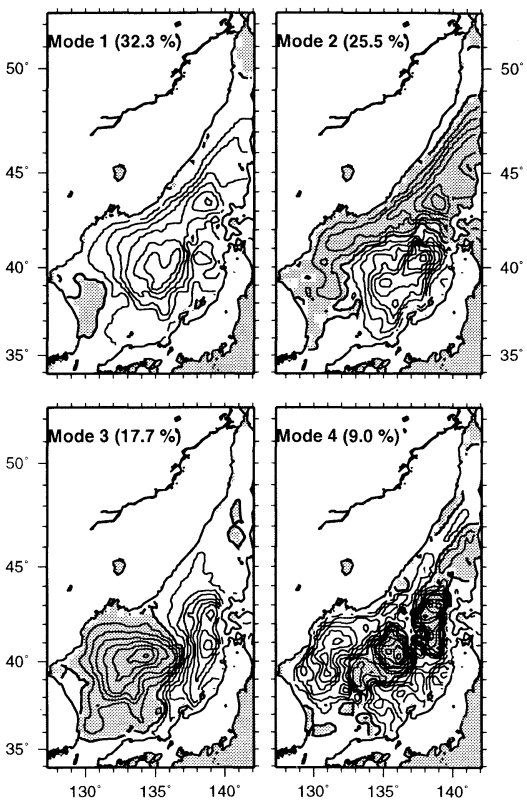

Fig. 14. Spatial patterns for first four TSF EOFs for the MM5 case. (Shaded area represents negative values)

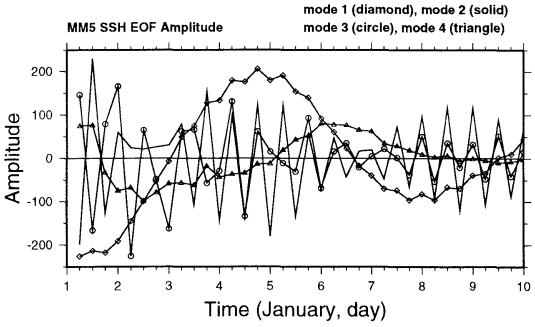

Fig. 13. Time-varying amplitudes (1 to 10 JAN 97) for first four SSH EOFs for the MM5 case.

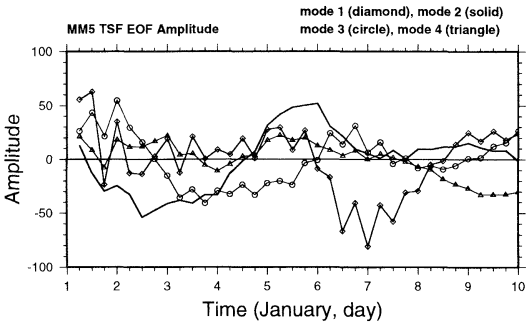

Fig. 15. Time-varying amplitudes (1 to 10 JAN 97) for first four TSF EOFs for the MM5 case.

(DRI) for the Japan (East) Sea (JES) of the U.S. Office of Naval Research. Dr. W. Timothy LIU, JPL provided the NSCAT wind analysis. Constructive comments by Academician Artem S. SARKISYAN, INM/RAS are gratefully acknowledged.

References

BANG, I., J. -K. CHOI, L.KANTHA, C.HORTON, M.CLIFFORD, M. -S. SUK, K. -I. CHANG, S. Y. NAM, and H. -J. LIE (1996): A hindcast experiment in the East Sea (Sea of Japan). La Mer, **34**: 108-130.

BLUMBERG, A. F. and G. L. MELLOR (1987): A

description of a three-dimensional coastal ocean circulation model. In: Three - Dimensional Coastal Ocean Models (Ed., N. S. HEAPS), Coastal and Estuarine Sciences, **4**: 1-16.

DUDHIA, J. (1993): A nonhydrostatic version of the Penn State-NCAR mesoscale model: Validation test and simulation of an Atlantic cyclone and cold front. Mon. Wea. Rev., **121**: 1493-1513.

KANG, H. S. (1997): Implementation, sensitivity testing, and evaluation of a numerical model for the East/Japan Sea circulation. University of Miami Technical Report, No. RSMAS-97-008, 174 numb. leaves.

KAWAMURA, H. and P. WU (1998): Formation mechanism of Japan Sea Proper Water in the flux center off Vladivostok. J. Geophys. Res., **103** (C10): 21, 611- 21,622.

LEVITUS, S. (1982): Climatological Atlas of the World Ocean. NOAA Prof. Paper 13, NOAA / ERL / GFDL, Princeton, NJ, 190 pp.

NA, J. -Y., J. -W. Seo and S. -K. Han (1992): Monthly mean sea surface winds over the adjacent seas of the Korea Peninsula. J. Oceanogr. Soc. Korea, **27**: 1-10.

SENJYU, T. and H. SUDO (1996): Interannual variation of the upper portion of the Japan Sea proper water and its probable cause. J. Oceanogr., **52**: 27-42.

SEUNG, Y. H. and J. H. YOON (1995): Some features of winter convection in the Japan East Sea. J. Oceanogr., **51**: 61-73.

Revised on February 5, 2000
Accepted on October 2, 2000